Coupling and pathway control of coenzyme Q redox state and respiration in isolated mitochondria

Timea Komlodi, Luiza HD Cardoso, Carolina Doerrier, Erich Gnaiger*

Oroboros Instruments, Innsbruck, Austria

* Corresponding author: erich.gnaiger@oroboros.at

Abstract

Redox states of mitochondrial coenzyme Q (mtCoQ or Q) reflect the balance between (*1*) reducing capacities of electron flow from fuel substrates converging at the Q-junction, (*2*) oxidative capacities downstream of Q to oxygen, and (*3*) the load on the OXPHOS system utilizing or dissipating the protonmotive force. A three-electrode sensor (Rich 1988; Moore et al 1988) was implemented into the NextGen-O2k to monitor the Q redox state continuously and simultaneously with oxygen consumption. The Q-Module was optimized for high signal-to-noise ratio and minimum oxygen diffusion. CoQ2 is added as a redox probe equilibrating with Q at Complexes CI, CII and CIII and the detecting electrode. Q-sensors are poised with the CoQ2 redox peak potentials determined by cyclic voltammetry, which provides quality control of the Q-sensor and reveals chemical interferences.

The Q redox state and oxygen consumption were measured simultaneously in isolated mitochondria. A coupling-control protocol was applied to analyze LEAK, OXPHOS, and electron transfer capacities (*L*, *P*, and *E*, respectively) in the succinate-pathway. In a second pathway-control protocol, NADH- and succinate-linked pathways (N and S) converge at the Q-junction. mtCoQ was more oxidized when O_2 flux was stimulated in coupling-control states with load increasing from *L* to *P* and *E*. In contrast, mtCoQ was more reduced when O_2 flux was stimulated with electron input capacities increasing from N-, S- to NS-pathway-control states. N- and S- pathway capacities were not completely additive, thus confirming partial pool behavior of Q as proposed in the plasticity model of supercomplex organization.

1. Introduction

The redox state of mitochondrial metabolites plays a central role in mitochondrial respiratory control. Analysis of oxygen consumption is one of the most established methods to study mitochondrial function in health and disease. High-resolution respirometry (HRR) is the state-of the art method to measure mitochondrial respiration in a wide variety of sample preparations with the application of substrate-uncoupler-inhibitor titration (SUIT) protocols (Doerrier et al 2018). Extension of HRR in the Oroboros Oxygraph-2k (O2k, Oroboros Instruments, Austria) with fluorometric or potentiometric methods allows simultaneous measurement of respiration and additional mitochondrial parameters (e.g. mitochondrial membrane potential, ATP synthesis, hydrogen peroxide production, Ca^{2+}, pH). The novel NextGen-O2k (Oroboros Instruments, Austria) is an all-in-one instrument which extends HRR with the amperometric measurement of the redox state of coenzyme Q (CoQ or Q) in the same experimental chamber, thus providing control and monitoring of the O_2 regime in the range of hyperoxia to anoxia, saving resources (time, biological sample, and reagents), and ensuring reproducibility and accuracy of the results.

Coenzyme Q (ubiquinone; 2,3-dimethoxy-5-methyl-6-polyprenyl-1,4-benzoquinone), was discovered in 1957 by Crane and colleagues. CoQ occurs in mitochondrial and other cellular membranes. It is a lipid composed of a benzoquinone ring with an isoprenoid side chain, two methoxy groups and one methyl group (Wolf et al 1958). Plastoquinones (2,3-dimethyl-1,4-benzoquinone) of the photosynthetic system have a similar structure, but the two methoxy groups are replaced by two methyl groups and do not present the methyl group in position five on the benzoquinone ring (Havaux 2020). The length of the isoprenoid chain depends on the species. The number *N* of isoprenoid units is indicated as CoQ*N*; for example, CoQ6 occurs in *Saccharomyces cerevisiae*, CoQ8 in *E. coli*, CoQ9 in *Caenorhabditis elegans* and rodents, CoQ10 in humans, and some species have more than one CoQ form, e.g. human and rodent mitochondria contain different proportions of CoQ9 and CoQ10 (Aber et al 1992; Aussel et al 2014; Awad et al 2018; Hernández-Camacho et al 2018; Watts, Ristow 2017).

CoQ is widely distributed among non-mitochondrial compartments (Morré, Morré 2011). In hepatocytes CoQ is located in the Golgi apparatus (Crane et al 1985; Nyquist et al 1970), peroxisomes (Turunen et al 2004), microsomes (Seshadri Sastry et al 1961), and the plasma membrane electron transport system (pMETS; review: Morré, Morré 2011). More than 30 % of the membrane-bound CoQ is extramitochondrial in rat liver (Kalén et al 1987; Morré, Morré 1989). Additionally, lysosomes have a redox chain comparable to mitochondria where CoQ acts as an electron carrier (Gille, Nohl 2000). Consequently, isolated mitochondria are the subject of our methodological study as the gold standard for selective measurement of the mitochondrial CoQ (mtCoQ) redox state.

CoQ is not only a key component of the mitochondrial electron transfer system ETS (Crane et al 1959; Hatefi et al 1959, Mitchell 1961), but also a functional marker of cell metabolism, including the protonmotive force *pmF* (Mitchell 1961, 1975), antioxidant capacity (Noh et al 2013), mitophagy (Rodríguez-Hernández et al 2009), and regulation

83 of the permeability transition pore (Balaban et al 2005; Bentinger et al 2007; Fontaine et
84 al 1998; Lopez-Lluch et al 2010). Several branches of the ETS converge at the Q-junction:
85 mtCoQ is reduced by electron supply from (*1*) mt-matrix dehydrogenases through
86 Complex I (CI), (*2*) fatty acid oxidation FAO via electron-transferring flavoprotein
87 Complex, (*3*) succinate through CII, (*4*) glycerophosphate through glycerophosphate
88 dehydrogenase Complex, (*5*) dihydro-orotate via dihydro-orotate dehydrogenase, and
89 from other enzyme complexes (Enriquez, Lenaz 2014; Gnaiger 2020). mtCoQ is oxidized
90 downstream through CIII, and electrons are subsequentially transferred via cytochrome
91 *c* to CIV and the terminal electron acceptor O_2.

92   The concept of the Q-cycle was proposed originally by Mitchell (1975) and was
93 elaborated further in several modifications, describing how CIII translocates hydrogen
94 ions against the *pmF* (Crofts 2004; Trumpower 1990; Trumpower, Gennis 1994). CoQ
95 exists in three different states: ubiquinone (oxidized), ubiquinol ($CoQH_2$, reduced), and
96 an intermediate semiquinone. $CoQH_2$ binds to the Q_o site of CIII, while ubiquinone binds
97 to the Q_i site of CIII. First, $CoQH_2$ reduces the iron-sulfur protein and loads cytochrome c_1
98 with one electron. The other electron is transferred to the b_L heme and reduces the b_H
99 heme, which transfers the electron to ubiquinone at the Q_i site, reducing it to a
100 semiquinone. A second $CoQH_2$ — oxidized at the Q_o site — is required to fully reduce this
101 semiquinone to ubiquinol at Q_i site. This results in two ubiquinols oxidized at the Q_o site
102 per one ubiquinone reduced at the Q_i site. In a full Q-cycle, four H^+ leave the mt-matrix
103 and enter the intermembrane space. The reduced cytochrome *c* transfers electrons
104 further to CIV. The ubiquinol generated at the Q_i site is recycled by binding to the Q_o site
105 of CIII (Hunte et al 2003; Trumpower 1990; Trumpower, Gennis 1994).

106   Kröger and Klingenberg analyzed the kinetic control of the CoQ redox state in
107 submitochondrial particles (Kröger, Klingenberg 1966, 1973a, 1973b). According to their
108 random collision model, at steady state the rate of reduction and oxidation of CoQ is
109 proportional to respiratory rate, and the redox-active Q-pool (80-90 % of total mtCoQ) is
110 homogenous (Ernster et al 1969; Gutman 1985; Kröger, Klingenberg 1966, 1973a, 1973b;
111 Lenaz 1988; Ragan and Cottingham 1985; Rich 1984; Hackenbrock et al 1986). However,
112 according to Gutman (1985) there is inhomogeneity of the Q-pool with different redox
113 states of CoQ at various reduction sites. Considering that lateral diffusion of CoQ is high
114 in the lipid bilayer and not rate-limiting for electron transfer, the inhomogeneity can be
115 explained by SCI$_n$III$_n$ supercomplex formation (NADH oxidation by CI) in contrast to the
116 free Q-pool between CII (and other dehydrogenases) and CIII (succinate oxidation)
117 (Bianchi et al 2004; Estronell et al 1992; Lenaz 1988; Rauchova et al 1997; Stoner et al
118 1984; Enriquez, Lenaz 2014). According to the solid model, CoQ intermediates are
119 transferred in the supercomplex by substrate channeling without equilibration with the
120 free Q-pool. The free Q-pool is a reservoir for binding to SCI$_n$III$_n$ and uncoupling proteins,
121 or for forming the permeability transition pore (Armstrong et al 2003; Bianchi et al 2003;
122 Echtay et al 2000; Lenaz, Genova 2009). The solid and random collision models are most
123 probably the extremes of a dynamic organization of mtCoQ, with intermediary states
124 described by the more recently developed plasticity model (Enriquez, Lenaz 2014).

125   Q-extraction is a well-established method for measurement of the Q redox state,
126 involving extraction of quinones and determination of the concentration of reduced and
127 oxidized quinones using high-performance liquid chromatography HPLC (Reed, Ragan
128 1987; Takada et al 1984; Van den Bergen et al 1994). It has the advantage that the
129 *concentrations* of specific quinones can be determined and some inhibitors can be used
130 which interfere with the Q-Module, e.g. benzohydroxamate. The disadvantages of this
131 technique are that (*1*) it is a time-consuming end-point assay which does not show real-
132 time and continuous profiles of the Q redox state, and (*2*) the amount of metabolically
133 inactive CoQ is not distinguished from the redox active Q-pool (Van den Bergen et al
134 1994).

135   In the present study, we describe the Q-Module of the NextGen-O2k, which allows
136 simultaneous measurement of O_2 consumption and the redox state of mtCoQ real-time in
137 isolated mitochondria.

138

2. Materials and methods

140

2.1. Reagents

142

143   Sigma Aldrich: MES hydrate: 2-(N-Morpholino)ethanesulfonic acid hydrate, cat. Nº
144 M8250; Ama: Antimycin A, cat. Nº A8674; ATP: adenosine 5'-triphosphate disodium salt
145 hydrate, cat. Nº A2383); BSA: fatty acid-free bovine serum albumin, cat. Nº A6003; $CaCO_3$:
146 calcium carbonate, cat. Nº C4830; CCCP: carbonyl cyanide 3-chlorophenylhydrazone
147 carbonate, cat. Nº C2759); CoQ2: cat. Nº C8081; D-sucrose: cat. Nº S7903; dithiothreitol:
148 cat. Nº D0632; EGTA: ethylene glycol tetra acetic acid, cat. Nº E4378; imidazole: cat. Nº
149 56750; HEPES: 2-[4-(2-hydroxyethyl)piperazin-1-yl]ethanesulfonic acid, cat. Nº H7523;
150 KCl: potassium chloride, cat. Nº 60130; KH_2PO_4: potassium dihydrogen phosphate, cat. Nº
151 P5655; KOH: potassium chloride, cat. Nº P1767; lactobionic acid: cat. Nº 153516; M:
152 malate, cat. Nº M1000; mannitol: cat. Nº M4125; $MgCl_2$: magnesium chloride, cat. Nº
153 M1028; phosphocreatine disodium salt: cat. Nº P7936; P: pyruvate, cat. Nº P2256; Rot:
154 rotenone, cat. Nº R8875; subtilisin: protease from *Bacillus licheniformis* Type VIII,
155 lyophilized powders, 7-15 mg/unit, cat. Nº P5380; S: succinate, cat. Nº S2378; sucrose:
156 cat. Nº S7903; taurine: cat. Nº T0625. — Calbiochem: ADP: adenosine 5'diphosphate
157 potassium salt, cat. Nº 117105. — Bartelt, Austria: EtOH: ethanol 99.9 %, cat. Nº
158 CL0005055000. — Scharlab: $MgCl_2 \cdot 6H_2O$: magnesium chloride hexahydrate, cat. Nº
159 MA0036. — Evoqua Water Technologies GmbH: deionized ultra-pure water (Ultra Clear™
160 TP UV UF TM). — Oroboros Instruments: MiR05-Kit: Product ID 60101-01.

161

2.2. Reagent preparation and storage

163

164   ADP (500 mM with 300 mM $MgCl_2 \cdot 6 H_2O$): weigh 501.3 mg ADP and add 1.2 mL H_2O.
165 Neutralize with 5 M KOH to dissolve ADP. Add 121.98 mg $MgCl_2 \cdot 6 H_2O$ and stir the
166 solution for 1-2 min at room temperature. Set the pH to 7 with 5 M KOH if necessary. Store
167 aliquots at -20 °C in plastic vials.

168   Antimycin A (5 mM): weigh 5.4 mg antimycin A in a small glass vial and add 2 mL
169 EtOH. Store aliquots at -20 °C in glass vials.

170   Biopsy preservation solution BIOPS: 2.77 mM CaK_2EGTA, 7.23 mM K_2EGTA, 20 mM
171   imidazole, 20 mM taurine, 50 mM MES, 0.5 mM dithiothreitol, 6.56 mM $MgCl_2 \cdot 6H_2O$, 5.77
172   mM ATP, 15 mM phosphocreatine disodium salt; pH 7.1 (Fontana-Ayoub et al 2016).

173   CaK_2EGTA: dissolve 2.002 g $CaCO_3$ in 100 mM hot solution of EGTA (7.608 g/200
174   mL distilled water), while stirring add 2.3 g KOH; adjust pH to 7.0. Store at -20 °C in Falcon
175   tubes.

176   CCCP (1 mM): dissolve 1.02 mg CCCP in 5 mL EtOH in a glass vial. Store aliquots at
177   -20 °C in dark glass vials.

178   CoQ2 (10 mM stock): dissolve one commercial vial of CoQ2 (2 mg) in 628 µL EtOH.
179   CoQ2 (1 mM stock): dilute 50 µL of the 10 mM CoQ2 stock with 450 µL EtOH in a dark
180   vial. Store aliquots at -20 °C in dark glass vials.

181   Isolation buffer A: 225 mM mannitol, 75 mM sucrose, 1 mM EGTA, 2.5 g/L BSA; pH
182   7.4. Dissolve 62.5 mg fatty acid free BSA in 50 mL suspension buffer (see below). Prepare
183   fresh each day. Isolation buffer B: Dissolve 5 mg subtilisin in 10 mL isolation buffer A.
184   Prepare fresh each day. Isolation buffer C: 320 mM sucrose, 10 mM Tris-Cl, 1 mM K-EDTA
185   and 2.5 g/L BSA; pH~7.4. Dissolve 0.25 g fatty acid free BSA in 250 mL isolation buffer D.
186   Prepare fresh each day. Isolation buffer D: 320 mM sucrose, 10 mM Tris-Cl, 1 mM K-EDTA;
187   pH~7.4. Dissolve 27.4 g sucrose, 0.303 g Tris-Cl, 0.093 g K-EDTA in 250 mL distilled
188   water. Adjust pH to 7.4. with KOH or HCl if needed. Store at -20 °C in Falcon tubes.

189   K_2EGTA: dissolve 7.608 g (100 mM) EGTA and 2.3 g (200 mM) KOH in 200 mL
190   distilled water; adjust pH 7.0 with KOH. Store at -20 °C in plastic vials.

191   M: Malate (400 mM): dissolve 268.2 mg malate in 3 mL H_2O. Set pH to 7.0 with 5 M
192   KOH and adjust volume to 5 mL. Store aliquots at -20 °C in plastic vials.

193   MiR05-Kit: 0.5 mM EGTA, 3 mM $MgCl_2 \cdot 6H_2O$, 60 mM lactobionic acid, 20 mM
194   taurine, 10 mM KH_2PO_4, 20 mM HEPES, 110 mM D-sucrose, 1 g/L BSA; pH 7.1 (Gnaiger et
195   al 2000).

196   P: Pyruvate (2 M): dissolve 44 mg P with 180 µL H_2O. Prepare fresh each day.

197   Rot: Rotenone (1 mM): dissolve 0.39 mg rotenone in 1 mL EtOH. Store aliquots at -
198   20 °C in dark glass vials.

199   S: Succinate (1 M): dissolve 1.3505 g succinate in 3 mL distilled water. Set pH to 7.0
200   with 1 M HCl and adjust final volume to 5 mL. Store aliquots at -20 °C in plastic vials.

201   Suspension buffer: 225 mM mannitol, 75 mM sucrose, 1 mM EGTA; pH 7.4. Dissolve
202   10.25 g mannitol, 6.42 g sucrose and 0.095 g EGTA in 250 mL distilled water. Adjust pH
203   to 7.4 with KOH or HCl if needed. Store at -20 °C in Falcon tubes.

204
205   *2.3. Animals*
206

207   C57 BL/6N wild-type young adult mice (male and female) were housed in clear
208   plastic cages (maximum five mice per cage) in the animal facility of the Medical University
209   of Innsbruck. Mice were kept in a controlled environment (22 °C, 12/12 h light/dark
210   cycle) and fed *ad libitum* with free access to water. After cervical dislocation, heart and
211   brain were removed and immediately placed in ice-cold BIOPS. All procedures involving

212 animals were conducted in accordance with the Austrian Animal Experimentation Act in
213 compliance with the European convention for the protection of vertebrate animals used
214 for experimental and other scientific purposes (Tierversuchsgesetz 2012; Directive
215 2010/63/EU; BMWFM-66.011/0128-WF/V/3b/2016). According to the 3Rs principle
216 the number of animals was minimized.
217
218 *2.4. Isolation of mitochondria*
219
220 A glass/Teflon potter (WiseStir HS-30E, Wisd laboratory instruments) and
221 centrifuge (Rotina 380R, Andreas Hettich GmbH & Co. KG, Tuttlingen, Germany) were
222 used. All procedures were carried out in an ice bath or at 4 °C.
223
224 Mouse heart mitochondria were isolated following Fontana-Ayoub et al (2015).
225 Briefly, wet mass of the whole heart was determined, washed with ice-cold BIOPS and
226 minced with scissors in ice-cold BIOPS (1 mL). The tissue was transferred into a pre-
227 cooled glass/Teflon potter and homogenized at ~1000 rpm (five strokes) in 2 mL
228 isolation buffer B. The homogenate was transferred to a 20-mL Falcon tube containing 3
229 mL isolation buffer B and centrifuged at 800 g for 10 min. Using a new 20-mL Falcon tube,
230 the supernatant was centrifuged at 10 000 g for 10 min. The supernatant was discarded,
231 the pellet was resuspended in isolation buffer A (final volume 2 mL), and centrifuged at
232 10 000 g for 10 min. The supernatant was discarded, and the mitochondrial pellet was
233 finally resuspended in 200 µL suspension buffer.
234
235 Mouse brain mitochondria were isolated following Sumbalova et al (2016). Briefly,
236 wet mass was determined, and the tissue was cut into small particles with a sharp scissor
237 in isolation buffer C. The medium was discarded, the tissue suspended in isolation buffer
238 C (0.1 g tissue/1 mL), transferred to a pre-cooled glass/Teflon potter, and homogenized
239 at 1000 rpm (five strokes). The homogenate was transferred to a 20-mL Falcon tube (0.5
240 g tissue/20 mL homogenate) and centrifuged at 1000 g for 10 min. The pellet was
241 discarded, and the supernatant was centrifuged at 6200 g for 10 min. The supernatant
242 was removed, the pellet resuspended in isolation buffer D (0.5 g tissue/10 mL), and
243 recentrifuged at 6200 g for 10 min. The supernatant was discarded, and the
244 mitochondrial pellet was finally suspended in 500 µL isolation buffer D.
245
246 The mitochondrial suspension was gently mixed with a 200-µL pipette (five up-
247 down cycles). Immediately afterwards, a 50-µL Hamilton syringe was used to inject the
248 mitochondrial suspension into the O2k-chamber through the titration capillary of the
249 stopper.
250
251 *2.5. Determination of mitochondrial protein content*
252
253 Mitochondrial protein content was determined based on Lowry et al (1951) using
254 the DC™ Protein Assay (Bio-Rad, Hercules, CA, US) following the manufacturer
255 instructions. The absorbance was measured at 620 nm in a Tecan Infinite TM F200
256 spectrophotometer (Tecan, Männedorf, Switzerland). 0.025 mg/mL isolated heart
257 mitochondria and 0.09 mg/mL isolated brain mitochondria were applied in the
258 experiments.
259

2.6. High-resolution respirometry

The O2k monitors the O_2 signal of polarographic oxygen sensors (POS) over time and plots O_2 consumption of a biological sample continuously. The O2k consists of two chambers which are designed to perform unlimited titrations during the measurement assay. The O2k allows simultaneous measurement of cell or mitochondrial (mt) respiration and other bioenergetic parameters for comprehensive OXPHOS analysis, e.g. mt-membrane potential, ATP synthesis, hydrogen peroxide production, Ca^{2+}, pH. The volume of the O2k-chamber was calibrated to 2 mL. Instrumental quality control was performed routinely as a standard operating procedure of HRR: (*1*) daily oxygen sensor test, and (*2*) monthly instrumental O_2 background test including zero calibration of the POS (Doerrier et al 2018; Gnaiger 2001; 2008). The medium is continuously stirred with a PEEK-coated magnetic stirrer bar at 750 rpm which provides optimum mixing of the sample in the medium and ensures a stable signal of the POS. The Q redox state and mitochondrial O_2 consumption were measured at 37 °C in respiration medium MiR05.

The volume-specific oxygen flux $J_{V,O2}$ [pmol·s^{-1}·mL^{-1}] is calculated real-time as the negative time derivative of the O_2 concentration by DatLab 7.4. The O_2 flux is corrected for (*1*) the instrumental O_2 background flux $J°_{O2}$, (*2*) dilution of the sample by titrations, and (*3*) residual oxygen consumption $J_{V,Rox}$ measured in the presence of isolated mitochondria without any respiratory fuel substrates and ADP or after inhibition of the electron transfer system.

O_2 flux and the Q-redox states were recorded and analyzed using DatLab 7.4 (Oroboros Instruments, Austria). CV was controlled and recorded using DatLab 8.0 (Oroboros Instruments, Austria). The dilution effect of titrations was also taken into account for Q redox fractions.

2.7. Q-Module

The Q-Module of the NextGen-O2k provides the basis for continuous monitoring of the redox state of CoQ in isolated mitochondria and chloroplasts (Figure 1). According to the original description (Rich 1988), a three-electrode system and a mobile short-chain CoQ mimetic (CoQ1 or CoQ2) are required to indirectly detect the redox state of the Q-pool trapped in the mitochondrial inner membrane mtIM. CoQ2 reacts both with the biochemical sites of the ETS and the measuring electrode. CoQ mimetics do not react directly with the long isoprenyl chain CoQ in the ETS, rather they are reduced by e.g. CI and CII and oxidized by CIII (Peter Rich, personal communication). If the redox state of the CoQ mimetic is in equilibrium with the redox state of CoQ in the ETS, the redox state of CoQ mimetic reflects the redox state of mtCoQ. In the present study, a low concentration of CoQ2 (1 µM) was used, as described by Moore et al (1991).

The three-electrode system consists of a glassy carbon electrode (GCE; working electrode), which is set at a fixed potential relative to the silver/silver chloride (Ag/AgCl) reference electrode (Rich 1988). The potential set on the GCE is chosen to be sufficient to either oxidize the reduced or reduce the oxidized CoQ2. A platinum (Pt) counter electrode completes the electronic circuit. If the GCE is set to a potential oxidizing CoQ2, then CoQ2

reduced by the biological system undergoes oxidation on the GCE surface, resulting in a current between the GCE and Pt electrodes. In this case the activity of the reduced CoQ2 is proportional to the current measured between GCE and Pt electrodes: the current increases in direct proportion to the activity of the reduced CoQ2. The current I [A] is converted into a voltage U (electric potential difference [V]) and amplified: $U=I \cdot R$ (R: resistance). Conversely, if the GCE is set to the CoQ2 reduction potential, the oxidized CoQ2 undergoes reduction on the GCE surface and current flows into the opposite direction. In the present study, the GCE was set to the oxidation peak potential E_{p1} when measuring the Q redox state. The GCE and Pt electrodes are built-in fixed parts of the Q-stopper, whereas the reference electrode can be inserted through a separate inlet (Figure 1).
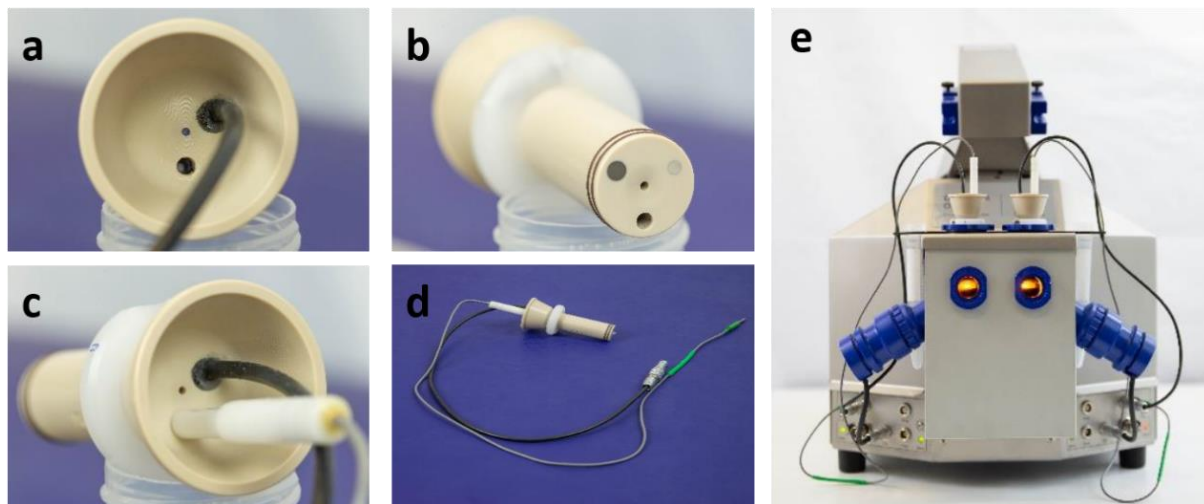
Figure 1. Q-sensor and stopper. The glassy carbon electrode (black) and platinum electrode (shiny silver) are built-in as fixed parts of the PEEK (polyether ether ketone) stopper. **(a)** Top view without reference electrode, showing the central gas-escape/titration capillary and the inlet for the reference electrode. **(b)** Bottom view without reference electrode, with conical center guiding gas bubbles to the capillary, double Viton O-rings. **(c)** Top view with reference electrode. **(d)** Q-sensor with reference electrode. **(e)** Q-stopper inserted into the chamber of the NextGen-O2k prototype (front view).

2.8.   Cyclic voltammetry

Cyclic voltammetry CV is used with the Q-Module to determine the oxidation and reduction peak potentials of the CoQ2 mimetic before the experiment and for quality control.

1. Clean the O2k-chamber three times for 5 min with H_2O. In the meantime, polish the Q-sensor with the built-in GCE and Pt electrodes with two different grades of aluminum oxide. First, polish the electrodes with 0.3 µm aluminum powder (use a few drops of H_2O) in a figure eight motion in a vertical position, then polish with the 0.05 µm aluminum powder in the same way. Afterwards, wash the Q-sensor with distilled water and rinse the reference electrode with water.

338   2. Add 2.3 mL MiR05 into the O2k-chamber. Insert the Q-stopper with the mounted
339   reference electrode into the O2k-chamber.
340   3. Determine the background CV with rotation of the stirrers set at 'off'. Titrate 30 µM (6
341   µL of 10 mM stock) CoQ2 into the chamber and switch on the stirrers to mix the CoQ2
342   solution with the medium. Switch the stirrers off and start CV to determine the
343   oxidation and reduction peak potentials. The parameters written in Section 3.2. for CV
344   are set automatically in the DatLab 8.0 software.
345   4. After CV, wash the O2k-chambers, stoppers, and reference electrodes with H_2O, 99.9
346   % EtOH, and H_2O again. Polish the GCE and Pt electrodes before the next use.
347
3.   Results

348
349
3.1.   Instrumental oxygen background test

350
351
352   The Q-stopper is equipped with the titration capillary, a large capillary for inserting
353   the reference electrode, and the fixed GC- and Pt-electrodes (Figure 1). The design was
354   optimized for minimum O_2 diffusion through the stopper, comparable with the
355   specifications of HRR using the standard O2k-stopper with a single injection capillary
356   (Gnaiger 2001).
357
358   Correction for instrumental background O_2 flux is a standard procedure in HRR
359   (Gnaiger 2001). The instrumental background O_2 flux is due to the O_2 consumption of the
360   POS, and O_2 diffusion into and out of the aqueous medium in the O2k-chamber, part of
361   which may occur through diffusion leaks in the stopper. The instrumental background O_2
362   flux $J°_{O_2}$ was measured in the absence of biological sample in the closed chamber in the
363   range of experimental O_2 levels at four different O_2 concentrations: near air saturation
364    $\sim$170 µM, $\sim$90 µM, $\sim$45 µM, $\sim$20 µM (Figure 2a). Each reduced O_2 level was obtained by
365   dithionite titrations using the TIP2k (Titration-Injection microPump), and maintained for
366   20 min. O_2 flux was a linear function of O_2 concentration. The intercept ($a°$: flux at zero
367   O_2 concentration) and slope ($b°$) were calculated from linear regressions for each
368   individual chamber. $a°$ was -2.6 ± 0.7 pmol·s^{-1}·mL^{-1} using the Q-stopper, not significantly
369   different from the intercept measured with the regular O2k-stoppers (-2.3 ± 0.4
370   pmol·s^{-1}·mL^{-1}; Figure 2b and c).

371
3.2.   Cyclic voltammetry

372
373
374   Cyclic voltammetry (CV) is applied as quality control to (*1*) determine the oxidation-
375   and reduction-peak potentials of CoQ2 under specific experimental conditions, (*2*) check
376   the quality of the Q-sensor, and (*3*) test the interference of chemicals used in the HRR
377   assay with the Q-sensor. In CV, the electrical potential between GCE and Ag/AgCl
378   electrodes is varied over time in cycles, while the current is recorded between the GC-
379   and Pt-electrodes. The current is plotted as a function of the applied electrical potential
380   in the cyclic voltammogram (Figure 3). In the voltammogram the characteristic peaks
381   refer to the maximum rate of CoQ2 oxidation (oxidation peak potential, E_{p1}) and to the
382   maximum rate of reduction (reduction peak potential, E_{p2}). These values are then used to
383   poise the GCE for monitoring the Q redox states with isolated mitochondria.
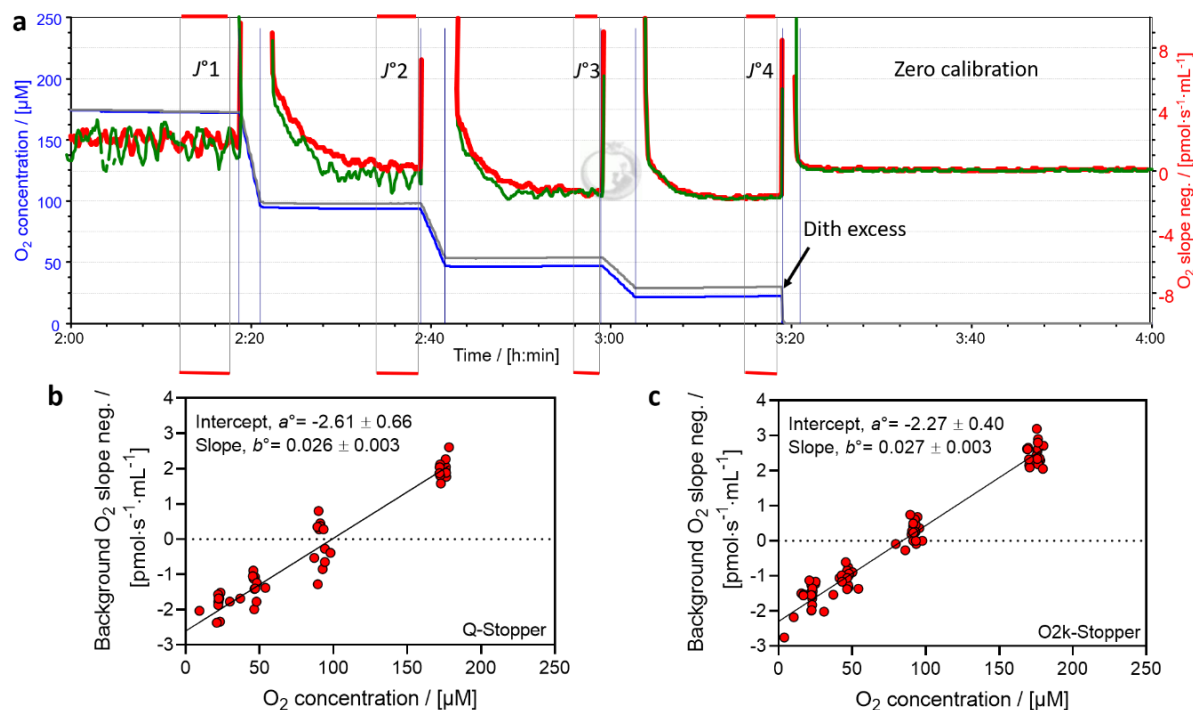
Figure 2. Instrumental O_2 background flux measured from air saturation to low oxygen in the NextGen-O2k using Q-stoppers and in the O2k with regular O2k-Stoppers. The O2 regime was controlled automatically using the TIP2k. **(a)** Superimposed traces of instrumental O_2 background tests measured in two experimental chambers using Q-stoppers. Blue plot: O_2 concentration [µM] in chamber A; grey plot: O_2 concentration [µM] in chamber B; red plot: volume-specific background O_2 flux [pmol·s^{-1}·mL^{-1}] in chamber A; green plot: volume-specific background O_2 flux [pmol·s^{-1}·mL^{-1}] in chamber B. $J°1$, $J°2$, $J°3$, and $J°4$ refer to background O_2 flux monitored at sequentially lowered O_2 concentrations. Excess dithionite (100 µL) was added to deplete the O_2 for zero calibration of the POS. Experiment 2019-08-28_PQ1-01. **(b) and (c)** Volume-specific background O_2 flux [pmol·s^{-1}·mL^{-1}] as a function of O_2 concentration measured at four different O_2 concentrations. Average ± SD were calculated for the intercept, $a°$, and the slope, $b°$, by linear regression for each individual chamber. Lines show linear regressions calculated through all data points. **b:** Measurement in 12 O2k-chambers of 5 instruments using different Q-stoppers. Experiments 2019-08-28_PQ1-01, 08-28_PQ2-01, 08-28_PQ3-01; 2020-04-21_PN2-01, 04-21_PQ2-01, 04-24_PN1-01. **c:** Measurement in 20 O2k-chambers with regular stoppers of 10 instruments. Experiments 2020-08-10_P2-01, 08-10_P3-01, 08-10_P9-01, 08-12_P1-01, 08-12_P5-01, 08-12_P6-01, 09-08_P4-01, 09-22_P10-01, 10-27_P7-01, 10-27_P8-01.

The following parameters are taken into account in CV:

- The initial polarization voltage is the potential applied at the start of CV. In order to avoid coating of the GCE, it must be close to the peak potential (Graham 2018). In the case of CoQ2, +30 mV was used as initial potential, which is close to the oxidation peak potential E_{p1}.

410 • Polarization window: The narrowest possible range of potentials should be applied
411 during CV scanning. Excessively high and low potentials might lead to chemical
412 modification or coating of the GCE (Graham 2018). Any type of coating of the GCE can
413 inhibit the electron transfer on the surface of it. In the case of CoQ2, -500 mV and +500
414 mV were chosen as a polarization window.
415 • Number of CV cycles: Although after one cycle (from -500 mV to +500 mV and back to
416 -500 mV) well-defined peaks for E_{p1} and E_{p2} are observed, it is recommended to run
417 more cycles to check whether additional peaks are detected or the shape of E_{p1} and E_{p2}
418 changes over the cycles owing to side-reactions. We found an optimum of five cycles in
419 standard CV applications.
420
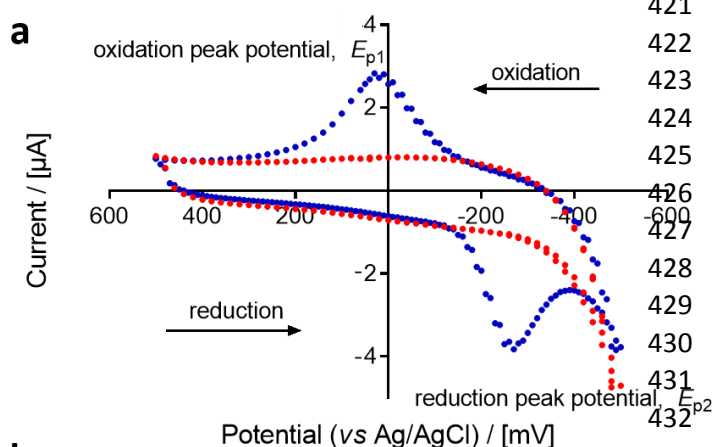
421 **Figure 3.** Cyclic voltammogram
422 in the absence and presence of 30
423 µM CoQ2 in non-stirred MiR05,
424 at 37 °C (NextGen-O2k). Initial
425 potential difference: +30 mV,
426 polarization window from -500
427 mV to +500 mV, scanning speed
428 100 mV/s, gain 1. **(a)** Red plot:
429 background CV without CoQ2;
430 blue plot: CV in the presence of
431 CoQ2; Experiment: 2019-06-
432 14_PQ2.
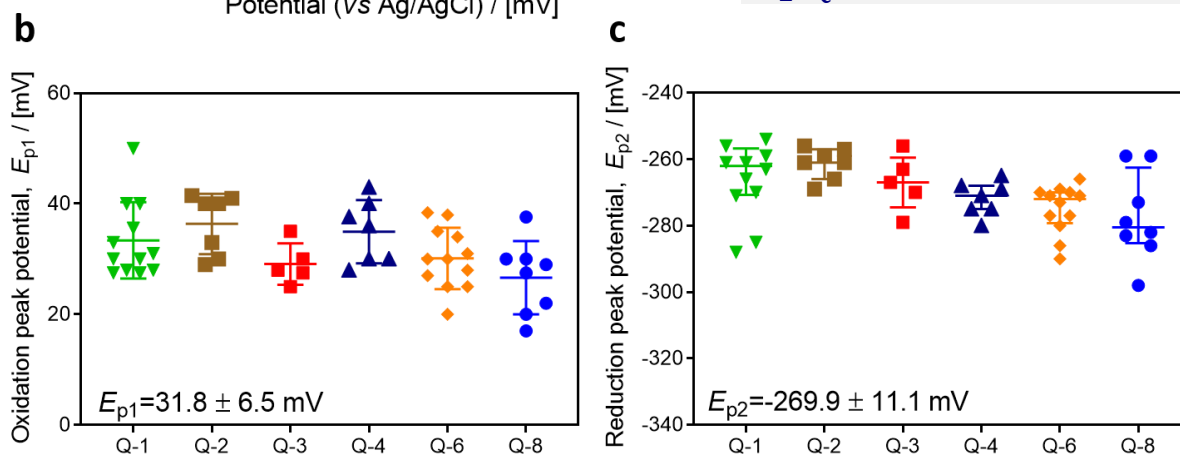
433 **(b)** Oxidation peak potential E_{p1} and **(c)** reduction peak potential E_{p2} of CoQ2 with six
434 different Q-sensors. E_{p1} and E_{p2} [mV] are shown as average ± SD; n=51.
435

436 • The scanning speed should allow for diffusion as the controlling process of exchange of
437 CoQ2 between the surface of GCE and the medium. If the scanning speed is very slow,
438 CoQ2 might be transported to and from the electrode surface via migration and
439 convection rather than diffusion (Graham 2018). If the scanning speed is too fast, it
440 leads to double layer charging current due to the rearrangement of solution molecules
441 at the surface of the GCE. This results in high baseline currents that obscures the

442   diffusion-controlled cyclic voltammogram (Graham 2018). 100 mV/s was applied as a
443   scanning speed.
444 • Stirring of the solution is avoided during CV to minimize convection. Upon stirring in
445   the presence of quinone (oxidized), only a peak related to quinone reduction is visible.
446   In contract, the peak of quinol oxidation cannot be observed, because the quinol is
447   stirred off from the surface of GCE (Peter R Rich, personal communication).
448 • The lowest concentration of CoQ2 should be applied which gives well-defined E_{p1} and
449   E_{p2}. In MiR05, 30 µM CoQ2 was optimal for CV, because lower CoQ2 concentrations did
450   not result in detectable peaks at gain 1 V/µA, whereas the limit of detection was
451   reached at higher than ~90 µM CoQ2.
452 • Temperature slightly influences the peak potentials; therefore, CV is performed at
453
454   experimental temperature.

455   CV serves as an essential quality control to evaluate the function of the Q-sensor. In
456 addition to the measurement of E_{p1} and E_{p2}, the shape of CV yields information on the
457 quality of electrodes, for avoiding drift and/or noise of the signal. No peaks should be
458 observed in the background CV without CoQ2, while the peaks in the presence of 30 µM
459 CoQ2 should be well-defined and sufficiently sharp (Figure 3). If the peaks are not sharp
460 enough and well-defined, or additional peaks are observed (with and without CoQ2), the
461 GCE and Pt electrodes are polished with aluminum powder, the Q-sensor and O2k-
462 chamber are washed with H_2O, 70 % ethanol, 99.9 % EtOH and H_2O, the glass barrel of
463 the reference electrode is filled with 3 M KCl solution, and the quality of the porous vycor
464 frit of the glass barrel of the reference electrode should be evaluated (Komlodi et al 2021).
465 Figure 3 shows E_{p1} and E_{p2} determined with CV after careful polishing of the GCE and Pt
466 electrode using different Q-sensors in various chambers of the NextGen-O2k. The E_{p1} of
467 CoQ2 was 31.8 ± 6.5 mV, and E_{p2} was -269.9 ± 11.1 mV using freshly polished electrodes.
468 Reproducibility of the CV measurements was high using different Q-sensors in various
469 NextGen-O2ks.
470
471 *3.3. Substrate-uncoupler-inhibitor titration protocols*
472
473   SUIT protocols are used to study respiratory control in different pathway- and
474 coupling-control states in a single experimental assay. A coupling-control protocol (SUIT-
475 006 Q mt D071) and a coupling-pathway control protocol (SUIT-031 Q mt D072) were
476 designed to investigate O_2 flux and the Q redox state simultaneously (Figure 4 and 5).
477 Harmonized SUIT protocols are developed with common cross-linked respiratory states,
478 which can be considered as replicate measurements and therefore, allow harmonization
479 of data obtained in different SUIT protocols. In SUIT-006 and SUIT-031 the harmonized
480 respiratory states are S(Rot)*P* and S(Rot)*E*. In chemical background tests, titrations in the
481 absence of mitochondria did not exert any effect on the Q signal in both SUIT protocols.
482

483 **Steps of the coupling-control protocol SUIT-006 (Figure 4):**
484
485 • After addition of isolated mitochondria and in the absence of any respiratory fuel
486   substrate and ADP, residual oxygen consumption *Rox* is due to the oxidative activity of
487   enzymes not related to the ETS. Addition of CoQ2 (1 µM).
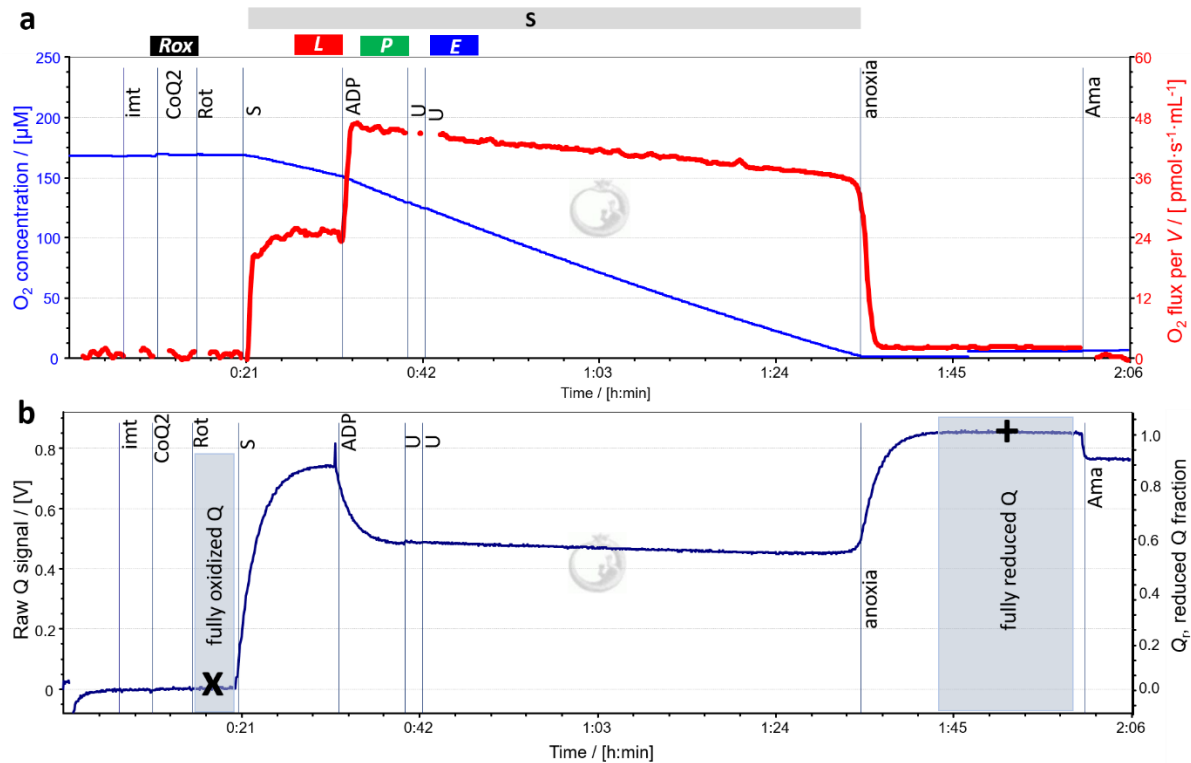
Figure 4: Coupling-control in the succinate-pathway S; SUIT-006. Simultaneous measurement of oxygen flux and Q redox state in mitochondria isolated from mouse heart. **(a)** Blue plot: O_2 concentration [μM]; red plot: O_2 flux per volume [pmol·s^{-1}·mL^{-1}]. **(b)** Non-calibrated (raw) Q signal [V] and reduced Q fraction Q_r. Fully oxidized Q ($Q_r = 0$) was calibrated in the presence of isolated mitochondria (imt), CoQ2, and rotenone (Rot); marked as x. Further titrations; S: S(Rot)-linked LEAK respiration L; ADP: S(Rot)-linked OXPHOS capacity P; U (uncoupler CCCP; 1 μM): S(Rot)-linked ET capacity E. Anoxia was used for calibration of fully reduced CoQ ($Q_r = 1$); marked as +. The effect of antimycin A (Ama) on the Q-signal could not be explained. Experiment: 2019-09-12_PQ1-02. **(c)** Coupling/pathway control diagram.

1. Rotenone (Rot; 0.5 μM) and Succinate (S; 10 mM): Rot inhibits respiration of endogenous substrates that remained after the mitochondrial isolation procedure. Additionally, rotenone avoids inhibition of succinate (S)-linked respiration caused by oxaloacetate accumulation (Gnaiger 2020). In the absence of rotenone, oxaloacetate is formed from malate in the reaction catalyzed by the NADH-dehydrogenase malate dehydrogenase (MDH) in the tricarboxylic acid (TCA) cycle. Rotenone inhibits CI and oxidation of NADH, which results in an increase of the NADH/NAD$^+$ ratio and consequently to feed-back inhibition of MDH and formation of oxaloacetate. Therefore, the S-linked OXPHOS capacity is measured in the presence of rotenone (Gnaiger 2020).

Succinate is a dicarboxylic acid formed in the TCA cycle and is the substrate of Complex II (CII). It is oxidized to fumarate and supports electron transfer through CII to the free mtCoQ-pool. Succinate with rotenone supports S-linked LEAK respiration and leads to maximal reduction of the Q-pool, reflected in the increase of the Q signal.

2. ADP (D; 2.5 mM) was added at kinetically saturating concentration to stimulate S-OXPHOS capacity and thus induce partial oxidation of the Q-pool. This was reflected in the decrease of the Q signal. To assess OXPHOS capacity, ADP was added at kinetically saturating concentration.

3. Uncoupler CCCP was titrated (U; 0.5 µM/step) to an optimum concentration for maximum flux as a measure of electron transfer capacity E. Neither O_2 flux nor the Q redox state changed after CCCP titrations, showing that OXPHOS capacity was not limited by the phosphorylation system.

4. Anoxia was reached after the mitochondria consumed the O_2 in the O2k-chambers. In the absence of O_2, the ETS is reduced and thus leads to full reduction of the Q-pool. Anoxia was used for calibration of fully reduced CoQ (Section 3.6.). Antimycin A (Ama; 2.5 µM) is a Q_i-site inhibitor of CIII and was added to check its effect on the fully reduced Q-pool under anoxia (Section 3.6.). The effect of Ama on the Q signal did not show dependence on the O_2 concentration (data not shown).

The steps of coupling-pathway control protocol SUIT-031 (Figure 5):

- Isolated mouse cardiac mitochondria; CoQ2 (1 µM).

1. Pyruvate & malate (PM; 5 mM P and 2 mM M) were added together to induce NADH-linked LEAK respiration. Pyruvate is converted to acetyl-CoA in the reaction catalyzed by pyruvate dehydrogenase. Malate serves as a co-substrate and after entering the mitochondria it is oxidized to oxaloacetate catalyzed by MDH. In both reactions NADH, the substrate of CI, is produced. Oxidation of NADH leads to reduction of the Q-pool through CI (Q signal increased). Interestingly, PM caused only partial reduction of the Q-pool compared to S(Rot) in the LEAK state in SUIT-006.

2. ADP (D; 2.5 mM) was added at kinetically saturating concentration to initiate N-OXPHOS capacity and thus, oxidize the Q-pool which is reflected in decrease of the Q signal.

3. Succinate (S; 10 mM) was added to induce NS-convergent electron transfer. Succinate further increased the O_2 flux and reduced the Q-pool in the OXPHOS state when added in the presence of PM, showing an additive effect in the Q-junction.

4. Rotenone (Rot; 0.5 µM) blocked N-linked respiration and led to oxidation of the Q-pool via CI inhibition leading to S-OXPHOS. The two protocols are harmonized at state S(Rot)$_P$.

5. Uncoupler CCCP (U; 0.5 µM/step) was titrated (1 µM in total) to initiate S-ET capacity which is a common respiratory state to SUIT-006, S(Rot)$_E$. Neither O_2 flux nor the Q redox state changed in mouse cardiac mitochondria showing that the S-OXPHOS capacity is not limited by the phosphorylation system.

6. Anoxia corresponds to the state where the Q-pool is fully reduced (Section 3.6.). Antimycin A (Ama; 2.5 µM).
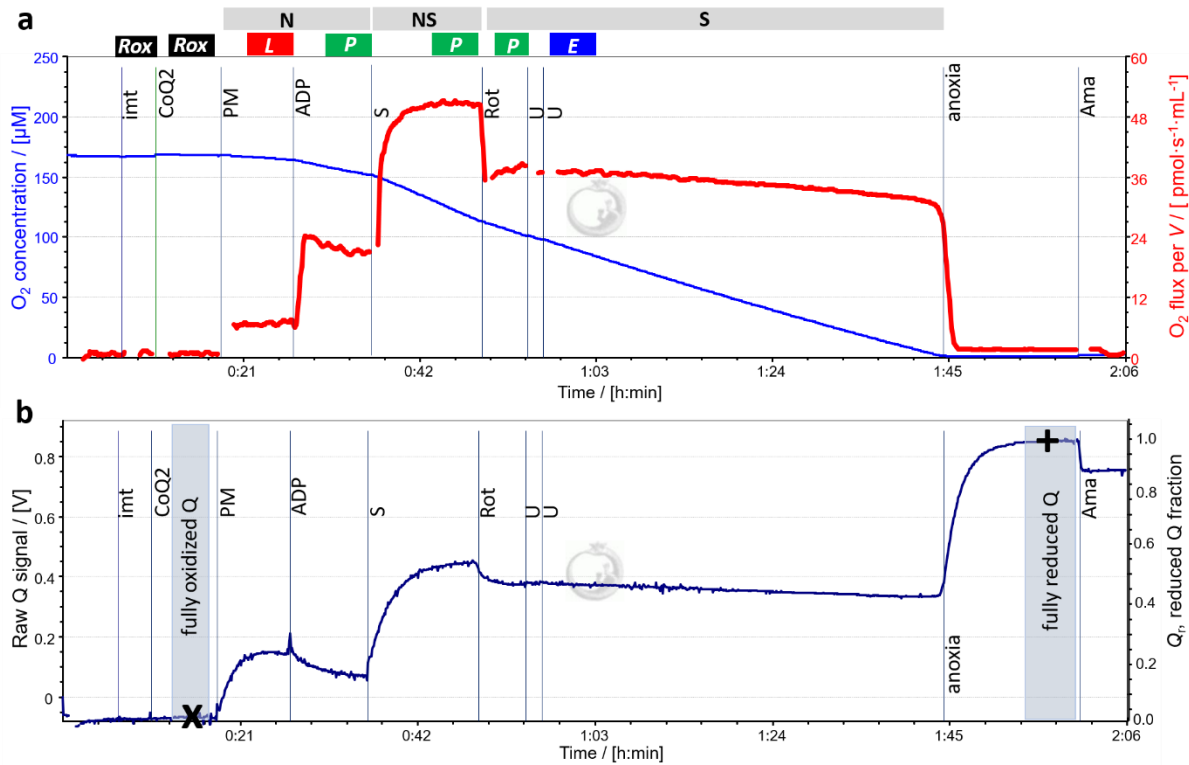
Figure 5: Pathway control in the N-, S-, and NS-pathways; SUIT-031. O₂ flux and Q redox state in mouse heart mitochondria. **(a)** Blue plot: O₂ concentration [μM]; red plot: O₂ flux [pmol·s⁻¹·mL⁻¹]. **(b)** Raw Q signal [V] and reduced Q fraction Q_r. Q_r = 0 calibrated in the presence of mitochondria (imt) and CoQ2 (x). Further titrations; PM (pyruvate & malate): N-linked LEAK respiration L; ADP: N-linked OXPHOS capacity P; S: NS-linked OXPHOS capacity P; Rot: S(Rot)-linked OXPHOS capacity P; U (uncoupler CCCP; 1 μM): S(Rot)-linked ET capacity E. Q_r = 1 calibrated under anoxia (+). Experiment: 2019-09-12_PQ1-02. **(c)** Coupling/pathway control diagram.

3.4. Q redox state

The Q redox state is expressed as the fraction of reduced Q (Q_r) in each steady state of a SUIT protocol. In order to calculate the reduced Q fraction, the raw Q signal (U_{raw}) is calibrated against the fully oxidized Q signal (U_{ox}) and the fully reduced Q signal (U_{red}). U_{ox} is measured in the presence of CoQ2 and isolated mitochondria. The CI inhibitor rotenone might have to be added to inhibit respiration of endogenous substrates (Section 3.5.). U_{red} is determined under anoxia after the sample consumed the accessible O₂ in the O2k-chamber (Section 3.6.). Q_r is calculated as a proportion of the fully reduced Q (Table

581 1). The sum of the oxidized and reduced fractions of Q equals 1, $Q_r + Q_{ox}$ = 1. In this
582 formalism the intermediate redox state of semiquinone is not taken into account.
583

584

Table 1. Calculation of the reduced Q fraction Q_r.

Symbol	Definition	Unit
U_{raw}	Raw (non-calibrated) Q signal	V
U_{red}	Fully reduced raw Q signal	V
U_{ox}	Fully oxidized raw Q signal	V
Q_{ox}	Calibrated fully oxidized Q $Q_{ox} = (U_{ox}-U_{ox})/(U_{red}-U_{ox}) = 0$ 100 % ubiquinone	-
Q_{red}	Calibrated fully reduced Q $Q_{red} = (U_{red}-U_{ox})/(U_{red}-U_{ox}) = 1$ 100 % ubiquinol	-
Q_r	Reduced Q fraction $Q_r = (U_{raw}-U_{ox})/(U_{red}-U_{ox})$	-

585
586   The use of two harmonized SUIT protocols (Figures 4 and 5) is required, when U_{ox} after
587 rotenone addition in SUIT-006 (Figure 4; S-pathway) is used for calibration in SUIT-031
588 (Figure 5; NADH-pathway).
589
590 *3.5.   Fully oxidized and reduced CoQ*
591
592   The fully oxidized and the fully reduced states of mtCoQ are obtained in the same
593 SUIT protocol for calibration. mtCoQ is fully oxidized in the presence of purified
594 mitochondria and CoQ2, and absence of any respiratory fuel substrates and ADP. CoQ2
595 may interact with non-mitochondrial Q-pools which may interfere with the Q signal in
596 crude isolated mitochondria. Mitochondria may contain endogenous substrates which
597 can slightly reduce mtCoQ in the calibration state for Q_{ox}. This was not the case in our
598 mitochondrial preparations as shown by the CI inhibitor rotenone not exerting any effect
599 on the Q signal and respiration (Figure 4).
600
601   The easiest and most calibration of fully reduced mtCoQ can be performed under
602 anoxia in the presence of biological sample. To do so, it is recommended to use a
603 concentration of sample which consumes relatively fast the O_2 in the closed chamber
604 leading to anoxia (more than 0.05 mg/mL; Figure 4 and 5). If limited amounts of sample
605 are available, the O_2 concentration can be decreased by nitrogen gas injection. CIV
606 inhibitors, i.e. azide and potassium cyanide, interfere with the Q-electrode.
607
608 *3.6.   Optimization of CoQ2 concentration*
609
610   Application of the lowest possible CoQ2 concentration is recommended to avoid any
611 side reaction on the ETS caused by the mimetics. Our study confirmed that 1 μM CoQ2
612 was sufficient to detect the redox states of mtCoQ without any influence on respiration.

The use of 0.5-1.5 µM CoQ2 did not influence the Q redox state measured at constant concentration of mouse heart mitochondria (Figure 6b). It is recommended to test the effect of CoQ2 on each type of mitochondria under experimental conditions.
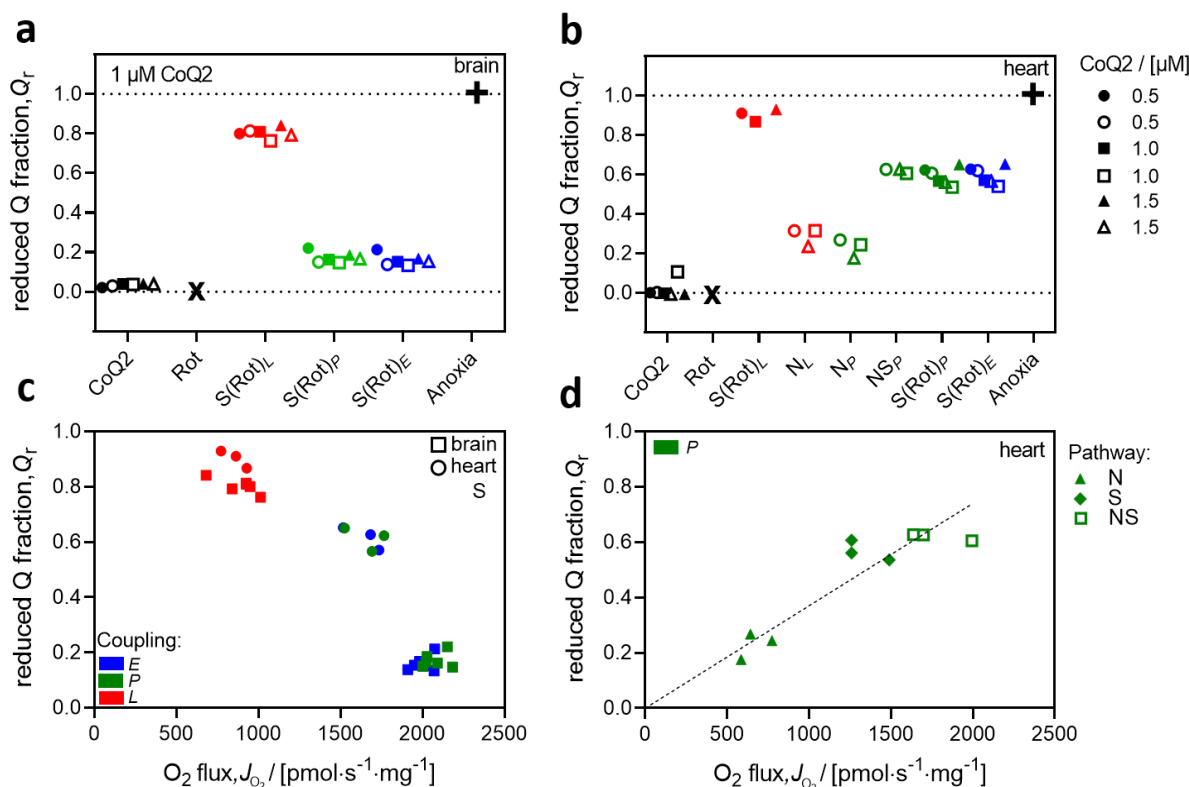
Figure 6: Reduced Q fraction (Q_r) and oxygen flux measured in mouse brain and heart mitochondria using six different Q-sensors. **(a)** Mouse brain with SUIT-006: Fully oxidized Q ($Q_r = 0$) was calibrated in the presence of isolated mitochondria (imt), CoQ2 (1 µM) and rotenone; marked as ✕. Respiratory states: S(Rot)-linked LEAK respiration S(Rot)$_L$; S(Rot)-linked OXPHOS capacity S(Rot)$_P$; S(Rot)-linked ET capacity S(Rot)$_E$. Anoxia was used for calibration of fully reduced CoQ ($Q_r = 1$); marked as ✚. Experiments: 2020-04-23_PN1-02; 2020-04-23_PN2-03; 2020-04-23_PQ2-02. **(b)** Mouse heart with SUIT-006 (filled symbols) and SUIT-031 (open symbols). Different CoQ2 concentrations were used as indicated. SUIT-031: Fully oxidized Q ($Q_r = 0$) was calibrated in the presence of imt, CoQ2 and rotenone; marked as ✕. Respiratory states: N-linked LEAK respiration N$_L$; N-linked OXPHOS capacity N$_P$; NS-linked OXPHOS capacity NS$_P$; S(Rot)-linked OXPHOS capacity S(Rot)$_P$; S(Rot)-linked ET capacity S(Rot)$_E$. Anoxia was used for calibration of fully reduced CoQ ($Q_r = 1$); marked as ✚. Experiments: 2019-09-12_PQ1-02; 2019-09-12_PQ2-03; 2019-09-12_PQ3-02. **(c)** Coupling control: effect of increased load — from LEAK- to OXPHOS- and ET-states — on Q_r as a function of O₂ flux per protein mass J_{O2} [pmol·s⁻¹·mg⁻¹] at constant S(Rot)-pathway state (from panels a and b). **(d)** Pathway control: effect of increased drive — with electron input into the Q-junction by separate or combined convergent pathways — on Q_r as a function of J_{O2} [pmol·s⁻¹·mg⁻¹] at constant OXPHOS-coupling state (from panel b). The intercept was not significantly different from zero, therefore, the regression line was forced through the origin.

3.7. Technical reproducibility

Figures 6 a and b show Q_r of technical replicates performed in parallel using different Q-sensors. In Figure 6a, the coupling-control protocol SUIT-006 was applied in mouse brain mitochondria (representative trace: Figure 4). In Figure 6b, both SUIT protocols (representative traces: Figure 4 and 5) were used with mouse heart mitochondria. The results indicate a high reproducibility in every pathway- and coupling- control states.

The use of a range of CoQ2 concentrations from 0.5 μM to 1.5 μM, keeping the same concentration of sample for every experimental chamber, did not impact the Q redox state (Figure 6). It is important, however, to keep the concentration of the CoQ mimetics used minimum to avoid affecting ETS.

3.8. Oxygen flux and reduced Q fraction

In the S-linked LEAK state, mtCoQ was highly reduced in brain (Q_r = 0.80 ± 0.02) and heart (Q_r = 0.90 ± 0.03; Figure 6a and b). In contrast, Q_r was lower (more oxidized) in the N-linked LEAK state (Q_r = 0.29 ± 0.04; Figure 6b).

At increased load downstream of the Q-junction by ADP-induced stimulation of respiration, mtCoQ became more oxidized in the OXPHOS state in brain (Q_r = 0.17 ± 0.03) and heart (Q_r = 0.61 ± 0.04; Figure 6c). In heart, Q_r was higher in the S-linked (Q_r=0.57 ± 0.03) than in the N-linked (Q_r=0.23 ± 0.04) OXPHOS state (Figure 6b and d). This is consistent with the high ET-capacity of the S- compared to the N-pathway (Figure 5). The higher electron supply capacity of the S-branch drives mtCoQ into a more reduced state. Uncoupling did not affect respiration and Q redox state in brain and heart, indicating that OXPHOS capacity is not limited by the ETS in these mitochondria. Whereas coupling control decreased Q_r (more oxidized) by increasing the load (higher flux; Figure 6c), pathway control increases Q_r (more reduced) by increasing the drive of electron input into the Q-junction (higher flux; Figure 6d). OXPHOS capacity in heart mitochondria was low in the N-pathway (CI-linked; J_N = 667 ± 79 pmol·s^{-1}·mg^{-1}), higher in the S-pathway (CII-linked; J_S = 1336 ± 109 pmol·s^{-1}·mg^{-1}), and showed an additive effect in the combined NS-pathway (J_{NS} = 1777 ± 156 pmol·s^{-1}·mg^{-1}). Q_r was directly proportional to the OXPHOS capacity under pathway control, increasing from 0.23 ± 0.04 (N), 0.57 ± 0.03 (S) to 0.58 ± 0.03 (NS) resulting in a linear dependence of Q_r on respiratory rate.

It is widely accepted that CII is not organized in a supercomplex and reacts with the free Q-pool, whereas the plasticity model suggests a large fraction of CI is organized as a supercomplex in junction with CIII and CIV (respirosome) with a tightly bound Q-pool. A direct link can be made between supercomplex channeling, Q-pool behaviour and additivity of NS-pathway capacity. Complete channeling through the supercomplex SCI$_n$-III$_n$-IV$_n$ predicts complete additivity ($A_{\widetilde{\alpha\beta}}$ = 1) obtained when the linear sum of the component N- and S-pathway ET capacities (J_N + J_S) equals the ET capacity of the convergent NS-pathway with the NS-substrate combination (J_{NS}). Without interaction between the redox components in the channel and the free redox intermediates, there is no interaction between the N- and S-pathways which implies complete additivity. The NS-linked O$_2$ flux (J_{NS}) was lower than J_N + J_S, pointing to incomplete additivity (Gnaiger

684 2020). In heart mitochondria, S was the dominant α-pathway with a higher flux J_S
685 compared to J_N. Flux control ratios are defined as $\alpha = J_S/J_{NS}$ and $\beta = J_N/J_{NS}$. Additivity $A_{\widetilde{\alpha\beta}}$
686 is defined as $(1-\alpha)/\beta$ (Gnaiger 2020). In heart, $A_{\widetilde{\alpha\beta}} = 0.66 \pm 0.02$ indicated incomplete NS-
687 additivity, which supports the plasticity model with partial Q-pool behavior.

4. Discussion

In the present work we optimized the simultaneous measurement of the Q redox state and respiration in isolated mitochondria using the amperometric three-electrode sensor.

4.1. Advantages

Real-time and continuous detection: Monitoring the mtCoQ redox state in real-time is one of the main advantages of this method in contrast to the Q-extraction method.

Simultaneous measurement of mtCoQ redox state and O₂ flux : The Q-Module integrated into the NextGen-O2k allows for simultaneous measurement of mtCoQ redox state and O_2 consumption in a closed chamber. Multiple titrations can be carried out via the titration/injection capillary of the specifically designed stopper, which closes the O2k-chamber.

Controlled O₂ concentrations and high resolution: Owing to the near air-tight experimental chamber, the O_2 concentration can be increased or decreased (between 0 and 1000 µM the POS gives a linear response), which allows measurement not only at air saturation, but also in hypoxic and hyperoxic ranges. Minimizing the O_2 diffusion is essential to obtain anoxic conditions for calibration at a fully reduced state. Using the original Q-electrode system (Rich 1988; Moore et al 1988; Dry et al 1989) resolution of the oxygen sensor was limited and oxygen diffusion into the closed chamber posed a problem, therefore, high mitochondrial concentrations were required.

Non-reducible Q-pool: According to Kröger, Klingenberg (1973b), 15-30 % of the total Q-pool is not reducible (not redox-active; Urban, Klingenberg 1969). This inactive Q-pool cannot interact with the Q-sensor, and thus does not interfere with evaluation of redox changes. If total CoQ is of interest, this would be a limitation, in which case the extraction method is advantageous (Van den Bergen et al 1994).

4.2. Limitations

Q-pool compartmentalization: CoQ2 does not interact with free mtCoQ, since it requires mediation by catalytically active respiratory Complexes participating in the Q-cycle and thus CoQ2 equilibrates with the mtCoQ pools that interact with the respiratory Complexes. CoQ compartmentalization occurs between a free CoQ pool in the lipid phase of the mtIM behaving according to the random collision model and a bound CoQ pool tightly associated with respiratory supercomplexes. CoQ compartmentalization needs to be considered in the interpretation of the amperometric signal of the Q-Module. This is particularly important if dissociation of supercomplexes is under control of the

protonmotive force *pmF*. Then equilibration of CoQ2 with compartmentalized mtCoQ relates to different pool sizes in the LEAK state at high *pmF* and the OXPHOS- and ET-states at lower and very low *pmF*, respectively (Figure 6). In this context it is interesting to note that uncoupler titrations inducing the transition from S(Rot)$_P$ to S(Rot)$_E$ did not affect the Q-redox state nor oxygen flux in the presence or absence of pyruvate&malate (Figures 4 and 5).

Determination of CoQ concentrations is not possible in contrast to the Q-extraction method.

Chemical interference: Some inhibitors and chemicals applied in HRR interfere and may even damage the Q-sensor. Dithionite, cytochrome *c*, ascorbate, TMPD (tetramethyl-p-phenylenediamine dihydrochloride), CIV inhibitors (i.e. potassium cyanide and azide) interfered with the Q signal. The alternative oxidase inhibitor benzohydroxamate and NADH cannot be applied with the Q-electrode (Van den Bergen et al 1994). We observed that cyclohexylammonium salts of some chemicals, e.g. glycerol-3-phosphate, disturb the Q signal. Thus, it is advisable to perform a chemical background test in the absence of biological sample, and CV (in the absence and presence of 30 µM CoQ2) to test for chemical interference with the Q-electrode. If the shape of the CV has changed or additional "peaks" in the current in CV are detectable, the questionable chemical cannot be used with the Q-electrode.

4.3. Conclusions

mtCoQ was more oxidized when O$_2$ flux increased under coupling control from LEAK- to OXPHOS- and ET-states (for terminology see Gnaiger et al 2020), but more reduced when O$_2$ flux was stimulated by electron supply under pathway control from N-, S-, to NS-pathway states. N- and S- pathway capacities showed incomplete additivity, which supports the plasticity model of supercomplex organization.

Amperometric monitoring of the Q redox state adds a new dimension to coupling- and pathway-control analysis of isolated mitochondria. The Q-Module enables real-time monitoring of the redox state of CoQ simultaneously with respiration. This is a powerful approach to expand studies in mitochondria physiology for a better understanding of mitochondria in health and disease.

Author contributions

EG and TK collaborated closely with WGT in the development of the Q-Module. TK and LHDC designed, carried out and analyzed the experiments. CD contributed to SUIT protocol development and commented on the manuscript. TK, LHDC and EG wrote the manuscript.

Conflicts of interest

EG is a founder and CEO of Oroboros Instruments, Innsbruck, Austria.

Data availability

Original files are available Open Access at Zenodo repository: 10.5281/zenodo.4478400

Abbreviations

Ama antimycin A; CCCP Carbonyl cyanide m-chlorophenyl hydrazone; CI Complex I, CII Complex II; CIII Complex III; CIV Complex IV; CoQ coenzyme Q; CV cyclic voltammetry; Dith dithionite; ET capacity electron transfer capacity; ETS electron transfer system; FAO: fatty acid oxidation; GCE glassy carbon electrode; HRR high-resolution respirometry; imt isolated mitochondria; M malate; Myx myxothiazol; N-linked NADH-linked pathway; OXPHOS oxidative phosphorylation; P pyruvate; POS polarographic oxygen sensor; Pt platinum; Q coenzyme Q; Rot rotenone; S succinate; SUIT substrate-uncoupler-inhibitor titration; TCA tricarboxylic acid; U uncoupler.

References

Aberg F, Appelkvist EL, Dallner G, Ernster L (1992) Disturbation and redox state of ubiquinones in rat and human tissues. Arch Biochem Biophys 295:230-4.

Armstrong JS, Whiteman M, Rose P, Jones DP (2003) The Coenzyme Q10 analog decylubiquinone inhibits the redox-activated mitochondrial permeability transition: role of mitcohondrial [correction mitochondrial] complex III. J Biol Chem 278:49079-84.

Aussel L, Pierrel F, Loiseau L, Lombard M, Fontecave M, Barras F (2014) Biosynthesis and physiology of coenzyme Q in bacteria. Biochim Biophys Acta, 1837:1004-11.

Awad AM, Bradley MC, Fernandez-Del-Rio L, Nag A, Tsui HS, Clarke CF (2018) Coenzyme Q10 deficiencies: pathways in yeast and humans. Essays Biochem 62:361-76.

Balaban RS, Nemoto S, Finkel T (2005) Mitochondria, oxidants, and aging. Cell 120(4):483-95.

Benard G, Faustin B, Galinier A, Rocher C, Bellance N, Smolkova K, Casteilla L, Rossignol R, Letellier T (2008) Functional dynamic compartmentalization of respiratory chain intermediate substrates: implications for the control of energy production and mitochondrial diseases. Int J Biochem Cell Biol 40:1543-54.

Bentinger M, Brismar K, Dallner G (2007) The antioxidant role of coenzyme Q. Mitochondrion 7 Suppl S41-50.

Bianchi C, Fato R, Genova ML, Parenti Castelli F, Lenaz G (2003) Structural and functional organization of Complex I in the mitochondrial respiratory chain. Biofactors 18:3-9.

Bianchi C, Genova ML, Parenti Castelli G, Lenaz G (2004) The mitochondrial respiratory chain is partially organized in a supercomplex assembly: kinetic evidence using flux control analysis. J Biol Chem 279:36562-9.

Crane FL, Hatefi Y, Lester RL, Widmer C (1957) Isolation of a quinone from beef heart mitochondria. Biochim Biophys Acta 1000:362-3.

Crane FL, Widmer C, Lester RL, Hatefi Y, Fechner W (1959) Studies on the electron transport system: XV. Coenzyme Q (Q275) and the succinoxidase activity of the electron transport particle. Biochim Biophys Acta 31:476-489.

Crane FL, Sun IL, Clark MG, Grebing C, Low H (1985) Transplasma-membrane redox systems in growth and development. Biochim Biophys Acta 811:233-64.

Crofts AR (2004) The cytochrome bc_1 complex: function in the context of structure. Annu Rev Physiol 66:689-733.

Doerrier C, Garcia-Souza LF, Krumschnabel G, Wohlfarter Y, Meszaros AT, Gnaiger E (2018) High-resolution FluoRespirometry and OXPHOS protocols for human cells, permeabilized fibers from small biopsies of muscle, and isolated mitochondria. Methods Mol Biol 1782:31-70.

Dry IB, Moore AL, Day DA, Wiskich JT (1989) Regulation of alternative pathway activity in plant mitochondria: nonlinear relationship between electron flux and the redox poise of the quinone pool. Arch Biochem Biophys 273:148-57.

Echtay KS, Winkler E, Klingenberg M (2000) Coenzyme Q is an obligatory cofactor for uncoupling protein function. Nature 408:609-13.

Enriquez JA, Lenaz G (2014) Coenzyme Q and the respiratory chain: coenzyme Q pool and mitochondrial supercomplexes. Mol Syndromol 5:119-40.

Ernster L, Lee IY, Norling B, Persson B (1969) Studies with ubiquinone-depleted submitochondrial particles. Essentiality of ubiquinone for the interaction of succinate dehydrogenase, NADH dehydrogenase, and cytochrome b. Eur J Biochem 9:299-310.

Estornell E, Fato R, Castelluccio C, Cavazzoni M, Parenti Castelli G, Lenaz G (1992) Saturation kinetics of coenzyme Q in NADH and succinate oxidation in beef heart mitochondria. FEBS Letters 311:107-9.

Fontaine E, Ichas F, Bernardi P (1998) A ubiquinone-binding site regulates the mitochondrial permeability transition pore. J Biol Chem 273:25734-40.

Fontana-Ayoub M, Krumschnabel G (2015) Isolation of mouse heart mitochondria. Mitochondr Physiol Network 20.06:1-2.

Fontana-Ayoub M, Fasching M, Gnaiger E (2016) Selected media and chemicals for respirometry with mitochondrial preparations. Mitochondr Physiol Network 03.02:1-10.

Gille L, Nohl H (2000) The existence of a lysosomal redox chain and the role of ubiquinone. Arch Biochem Biophys 375:347-54.

Gnaiger E (2001) Bioenergetics at low oxygen: dependence of respiration and phosphorylation on oxygen and adenosine diphosphate supply. Respir Physiol 128:277-97.

Gnaiger E (2008) Polarographic oxygen sensors, the oxygraph and high-resolution respirometry to assess mitochondrial function. In: Mitochondrial Dysfunction in Drug-Induced Toxicity (Dykens JA, Will Y, eds) John Wiley & Sons, Inc, Hoboken, NJ:327-52.

Gnaiger E (2020) Mitochondrial pathways and respiratory control. An introduction to OXPHOS analysis. 5th ed. Bioenerg Commun 2020.2:112 pp.

Gnaiger E et al — MitoEAGLE Task Group (2020) Mitochondrial physiology. Bioenerg Commun 2020.1:44 pp.

Gnaiger E, Kuznetsov AV, Schneeberger S, Seiler R, Brandacher G, Steurer W, Margreiter R (2000) Mitochondria in the cold. In: Life in the Cold (Heldmaier G, Klingenspor M, eds) Springer, Heidelberg, Berlin, New York:431-42.

Graham DJ (2018) Standard operating procedures for cyclic voltammetry. 126 pp. ISBN: 978-1387514304.

Gutman M (1985) Kinetic Analysis of electron flux through the mitochondrial system. Coenzyme Q, Chichester, UK: Wiley 10: 215-234.

Komlodi T et al (2021) MitoFit Preprints 2021.2

877   Hackenbrock CR, Chazotte B, Gupte SS (1986) The random collision model and a critical
878   assessment of diffusion and collision in mitochondrial electron transport. J Bioenerg
879   Biomembr 18:331–368.
880   Hatefi Y, Lester RL, Crane FL, Widmer C (1959) Studies on the electron transport system. XVI.
881   Enzymic oxidoreduction reactions of coenzyme Q. Biochim Biophys Acta 31:490-501.
882   Havaux M (2020) Plastoquinone in and beyond Photosynthesis. Trends Plant Sci 25:1252-1265.
883   Hernández-Camacho JD, Bernier M, López-Lluch G, Navas P (2018) Coenzyme Q(10)
884   Supplementation in Aging and Disease. Frontiers in physiology 9:44.
885   Hunte C, Palsdottir H, Trumpower BL (2003) Protonmotive pathways and mechanisms in the
886   cytochrome bc1 complex. FEBS Lett 545:39-46.
887   James AM, Cochemé HM, Smith RAJ, Murphy MP (2005) Interactions of mitochondria-targeted
888   and untargeted ubiquinones with the mitochondrial respiratory chain and reactive oxygen
889   species. Implications for the use of exogenous ubiquinones as therapies and experimental
890   tools. J Biol Chem 280:21295-312.
891   Kalén A, Appelkvist EL, Dallner G (1987) Biosynthesis of ubiquinone in rat liver. Acta Chem Scand
892   B 41:70-2.
893   Komlodi T, Cardoso LHD, Gollner M, Merth A, Hunger M, Iglesias-Gonzalez J, Doerrier C, Tindle-
894   Solomon L, Schwaninger H, Walter-Vracevic M, Gradl P, Moore AL, Gnaiger E (2021)
895   NextGen-O2k: Q-Module manual. Mitochondr Physiol Network 24.12:1-21.
896   Kröger A, Klingenberg M (1966) On the role of ubiquinone in mitochondria. II. Redox reactions of
897   ubiquinone under the control of oxidative phosphorylation. Biochem Z 344:317-36.
898   Kröger A, Klingenberg M (1973a) The kinetics of the redox reactions of ubiquinone related to the
899   electron-transport activity in the respiratory chain. Eur J Biochem 34: 358-68.
900   Kröger A, Klingenberg M (1973b) Further evidence for the pool function of ubiquinone as derived
901   from the inhibition of the electron transport by antimycin. Eur J Biochem 39:313-23.
902   Lenaz G (1988) Role of mobility of redox components in the inner mitochondrial membrane. J
903   Membr Biol 104:193-209.
904   Lenaz G, Genova ML (2009) Structural and functional organization of the mitochondrial
905   respiratory chain: A dynamic super-assembly. Int J Biochem Cell Biol 41:1750-72.
906   Lopez-Lluch G, Rodriguez-Aguilera JC, Santos-Ocana C, Navas P (2010) Is coenzyme Q a key factor
907   in aging? Mech Ageing Dev 131:225-35.
908   Lowry OH, Rosebrough NJ, Farr AL, Randall RJ (1951) Protein measurement with the Folin phenol
909   reagent. J Biol Chem 193:265-75.
910   Mitchell P (1961) Coupling of phosphorylation to electron and hydrogen transfer by a chemi-
911   osmotic type of mechanism. Nature 191:144-8.
912   Mitchell P (1975) The protonmotive Q cycle: A general formulation. FEBS Lett 59:137-9.
913   Moore AL, Dry IB, Wiskich TJ (1988) Measurement of the redox state of the ubiquinone pool in
914   plant mitochondria. FEBS Lett 235:76-80.
915   Moore AL, Dry IB, Wiskich JT (1991) Regulation of electron transport in plant mitochondria under
916   State 4 Conditions. Plant Physiol 95:34-40.
917   Morré DJ, Morré DM (1989) Preparation of mammalian plasma membranes by aqueous two-
918   phase partition. Biotechniques 7:946-958.
919   Morré DJ, Morré DM (2011) Non-mitochondrial coenzyme Q. Biofactors 37:355-60.
920   Noh YH, Kim K-Y, Shim MS, Choi S-H, Choi S, Ellisman MH, Weinreb RN, Perkins GA, Ju W-K (2013)
921   Inhibition of oxidative stress by coenzyme Q10 increases mitochondrial mass and improves
922   bioenergetic function in optic nerve head astrocytes. Cell Death Dis 4:e820.
923   Nyquist SE, Barr R, Morré DJ (1970) Ubiquinone from rat liver Golgi apparatus fractions. Biochim
924   Biophys Acta 208:532-4.

Ragan CI, Cottingham IR (1985) The kinetics of quinone pools in electron transport. Biochim Biophys Acta 811:13-31.

Rauchová H, Fato R, Drahota Z, Lenaz G (1997) Steady-state kinetics of reduction of coenzyme Q analogs by glycerol-3-phosphate dehydrogenase in brown adipose tissue mitochondria. Arch Biochem Biophys 344:235-41.

Reed JS, Ragan CI (1987) The effect of rate limitation by cytochrome c on the redox state of the ubiquinone pool in reconstituted NADH: cytochrome c reductase. Biochem J 247:657-62.

Rich PR (1984) Electron and proton transfers through quinones and cytochrome *bc* complexes. Biochim Biophys Acta 768:53-79.

Rich PR (1988) Patent of Q-electrode. Monitoring membrane bounded systems. Glynn Res. Ph., Bodmin; European Patent Nº85900699.1.

Rodríguez-Hernández A, Cordero MD, Salviati L, Artuch R, Pineda M, Briones P, Izquierdo LG, Cotán D, Navas P, Sánchez-Alcázar JA (2009) Coenzyme Q deficiency triggers mitochondria degradation by mitophagy. Autophagy 5:19-32.

Seshadri Sastry P, Jayaraman J, Ramasarma T (1961) Distribution of coenzyme Q in rat liver cell fractions. Nature 189:577.

Stoner CD (1984) Steady-state kinetics of the overall oxidative phosphorylation reaction in heart mitochondria. Determination of the coupling relationships between the respiratory reactions and miscellaneous observations concerning rate-limiting steps. J Bioenerg Biomembr 16:115-41.

Sumbalova Z, Fontana M, Krumschnabel G (2016) Isolation of rat brain mitochondria. Mitochondr Physiol Network 20.07:1-2.

Takada M, Ikenoya S, Yuzuriha T, Katayama K (1984) Simultaneous determination of reduced and oxidized ubiquinones. Methods Enzymol 105:147-55.

Trumpower BL (1990) The protonmotive Q cycle. Energy transduction by coupling of proton translocation to electron transfer by the cytochrome bc1 complex. J Biol Chem 265:11409-12.

Trumpower BL, Gennis RB (1994) Energy transduction by cytochrome complexes in mitochondrial and bacterial respiration: the enzymology of coupling electron transfer reactions to transmembrane proton translocation. Annu Rev Biochem 63:675-716.

Turunen M, Olsson J, Dallner G (2004) Metabolism and function of coenzyme Q. Biochim Biophys Acta 1660:171-99.

Urban PF, Klingenberg M (1969) On the redox potentials of ubiquinone and cytochrome b in the respiratory chain. Eur J Biochem 9:519-25.

Van den Bergen CW, Wagner AM, Krab K, Moore AL (1994) The relationship between electron flux and the redox poise of the quinone pool in plant mitochondria. Interplay between quinol-oxidizing and quinone-reducing pathways. Eur J Biochem 226:1071-8.

Watts JL, Ristow M (2017) Lipid and carbohydrate metabolism in *Caenorhabditis elegans*. Genetics 207:413-46.

Wolf DE, Hoffman CH, Trenner NR, Arison BH, Shunk CH, Linn BO, McPherson JF, Folkers K (1958) Coenzyme Q. I. Structure studies on the coenzyme Q group. J Am Chem Soc 80:4752.

Wu F, Yang F, Vinnakota KC, Beard DA (2007) Computer modeling of mitochondrial tricarboxylic acid cycle, oxidative phosphorylation, metabolite transport, and electrophysiology. J Biol Chem 282:24525-37.